Spatio-temporal pattern formation during CO oxidation on Pt(100) at low and intermediate pressures: A comparative study

T. Lele and J. Lauterbach[a)]
School of Chemical Engineering, Purdue University, West Lafayette, Indiana 47906-1283

(Received 13 July 2001; accepted 3 December 2001; published 21 February 2002)

Experimental studies of CO oxidation on Pt(100) over two different ranges of reactant pressures will be reviewed. Using photoemission electron microscopy (PEEM), spatio-temporal pattern formation was observed at temperatures between 420 and 540 K in the 10^{-5} mbar pressure range. In an attempt to bridge the ''pressure-gap,'' ellipsomicroscopy for surface imaging was used to follow pattern formation at temperatures around 600 K in the 10^{-2} mbar pressure range. The features of the nonlinear phenomena, observed in these two different pressure regimes, are markedly different. This is shown by comparison of various qualitative and quantitative features of spatio-temporal pattern formation as well as the dynamics of the macroscopic reaction rate. Subsurface oxygen is proposed as a tentative alternative to the surface phase transition for oscillations in the reaction rate at higher temperatures and intermediate pressures. © *2002 American Institute of Physics.*
[DOI: 10.1063/1.1446422]

This article reviews experimental studies directed toward elucidating spatio-temporal pattern formation in a nonlinear heterogeneous catalytic reaction, in this case CO oxidation on a well-defined Pt(100) single crystal. Two different types of imaging tools have been used, one at low pressures called the photoemission electron microscope (PEEM), and the other at intermediate pressures, called ellipsomicroscopy for surface imaging (EMSI). The focus is on studying spatio-temporal pattern formation and its correlation to the integral reaction rate over a wide variety of pressures. It is shown that there is a marked difference between phenomena going from lower to intermediate pressures, thus making the case for active future study at atmospheric and higher pressures.

I. INTRODUCTION

CO oxidation is the most widely studied model reaction on single crystal catalysts.[1] The reaction follows a simple Langmuir–Hinshelwood mechanism.[2] However, amazingly complex nonlinear behavior has been observed during the course of the reaction, in the form of dynamic concentration patterns of CO and oxygen (spatio-temporal pattern formation) as well as macroscopic reaction rate oscillations on different low index single crystals and polycrystalline foils.[1,3–7] The origins of this complex behavior are believed to lie in the coupling of adsorption, desorption, and chemical reaction (as given by the Langmuir–Hinshelwood mechanism) with one of the following physical phenomena: (i) an adsorbate induced surface phase transformation,[8–11] (ii) oxide formation[12] and (iii) subsurface oxygen formation.[13–15] Single crystal surfaces like Pt(111), for example, exhibit purely bistable behavior; they do not show self-sustained pattern formation because none of the three above-mentioned driving forces are present for this surface. The Pt(100) surface, on the other hand, exists in two different configurations depending on the surface concentration of adsorbed chemical species.[9,16,17] Below a critical value of CO coverage, the surface dynamically reconstructs to a quasi-hexagonal 5×20 configuration, while above the critical value, the reconstruction is lifted to form a 1×1 structure.[16,18] Lower heat of adsorption on the 1×1 surface is the driving force for this surface phase transformation. The kinetics of the Pt(100) phase transition has been investigated using molecular beam studies,[19–21] and a power law model has been suggested to model the process.

The adsorption probability of oxygen on the hex surface is less than 0.001, while that on the 1×1 phase is around 0.1.[18] This is what mainly differentiates Pt(100) from other reconstructing surfaces like Pt(110), where the difference in adsorption probabilities of oxygen between the 1×1 and 1×2 phases in Pt(110) is only about 50% (apart from the obvious fact that the kinetics of the phase transformation are different). As a result, pattern formation on Pt(100) is strikingly different from Pt(110); waves, for example, have not been observed on Pt(100).[22,23] The surface phase transformation also facilitates the formation of subsurface oxygen on Pt(100).[13] A microscopic model for the formation of subsurface oxygen, using the fact that the surface undergoes phase transformation occurs on Pt(100), has been proposed.[13]

II. HISTORICAL PERSPECTIVE

Rate oscillations during CO oxidation have been extensively studied using a variety of techniques. Early efforts focused on monitoring oscillations in the work function in real time using a Kelvin probe.[24] Scanning low energy electron diffraction (LEED) measurements coupled with Kelvin probe measurements suggested that the oscillations in the work function were strongly correlated to periodic changes of the surface structure between the 1×1 and the hex

a)Author to whom correspondence should be addressed; Electronic mail: jochen@ecn.purdue.edu

phase.[9,25] With the invention of the PEEM, it became possible to image and distinguish between CO and oxygen covered areas (the contrast between the two adsorbates is again caused by differences in the work function).[26–28] PEEM led to the discovery of dynamic pattern formation on the catalyst surface. With the advent of the PEEM, a new species called subsurface oxygen was discovered during pattern formation, especially at temperatures in excess of 550 K, and its presence was confirmed using Auger electron spectroscopy.[14] Methods were developed to form subsurface oxygen in a controlled manner, and its reactivity toward CO, hydrogen, and oxygen was studied.[13] We believe that subsurface oxygen could play an important role during rate oscillations that exist at higher temperatures and pressures. PEEM however, cannot be operated above pressures of $\sim 10^{-4}$ mbar, owing to the fact that it relies on the usage of electrons. This led to a pressure gap between pattern formation studies at lower pressures and higher pressures. Recently, due to the development of two imaging techniques, ellipsomicroscopy for surface imaging (EMSI) and reflection anisotropy microscopy (RAM), it became possible to image patterns at arbitrary pressures.[3,29–33] Recent experiments at pressures of 0.1 mbar involving imaging using EMSI and postreaction Auger electron spectroscopy and thermal desorption spectroscopy have revealed the formation of an oxide species, different from subsurface oxygen.[34]

In this article, we present a review of the experimental studies that have been performed with PEEM and EMSI on CO oxidation on Pt(100). In the experimental section, we first briefly introduce the two experimental setups that have been used in the studies. This will be followed by experimental observations using PEEM and EMSI at both low and high pressures and comparisons thereof, with respect to qualitative similarities and differences in nonlinear behavior. Subsurface oxygen formation and its role during oscillations at intermediate pressures will also be briefly discussed.

III. EXPERIMENT

Our experiments are motivated by trying to understand and correlate spatio-temporal pattern formation on the Pt(100) single crystal surface with macroscopic behavior of the reaction rate. PEEM and EMSI are used to follow, in real time, pattern formation on micron length scales. The details of the principle of operation and the setup of these instruments are available elsewhere.[3,27,31,35] We outline below our experimental setup, and briefly mention some details about EMSI and PEEM.

A. EMSI setup (Purdue University)

The main chamber is a stainless steel ultrahigh vacuum system pumped to a base pressure below 1×10^{-10} mbar. It is equipped with an Auger electron spectrometer and a differentially pumped quadrupole mass spectrometer along with an ion gun for argon ion sputtering. CO oxidation is carried out in a small stainless steel reactor, which is connected to the main chamber via a straight-through metal seal valve. Product sampling is performed by leaking the reactor exit stream into the differentially pumped mass spectrometer head. A transfer rod is used to transfer the sample with sample mount from the reactor to the manipulator in the main chamber and back.[36] The Pt(100) single crystal is mounted vertically in the reaction cell on a combination of linear and rotary feed-through, which serves as the sample manipulator. Pressure measurement in the reactor is performed via a capacitance manometer gauge from 10^{-5} to 10^{-1} mbar and a convectron gauge from 10^{-2} mbar to atmospheric pressure. Two 2.75 in. quartz conflat windows are located on opposite sides of the cube to provide access for the EMSI. The reactor is evacuated with a 70 L/s turbo pump backed by a 250 L/s rotary vane mechanical pump. The total reactor volume is approximately 0.5 L. A gas manifold with three mass flow controllers is used to regulate the gas flow rates. The reactor pressure is controlled by a MKS 600 series pressure controller, which takes input from the capacitance manometer gauge, and operates a butterfly valve operating above the turbo pump. This system allows for independent control of the system pressure, gas composition, and mass flow rates.

The Pt(100) single crystal used was 1 cm in diameter. The same crystal was used for the high- and low-pressure experiments. The crystal typically underwent argon ion sputtering for 15 min at an argon pressure of 5×10^{-4} mbar, followed by annealing to 1200 K. Next, the sample temperature was cycled several times between 500 and 900 K in the presence of 5×10^{-5} mbar oxygen. Analysis of the surface chemical composition was frequently performed using auger electron spectroscopy (AES) to verify the absence of any contaminants on the surface.

EMSI makes use of an ellipsometer, which is coupled with lenses and a CCD detector; the latter makes it possible to obtain spatially resolved information. The imaging ellipsometer is sensitive to sub-monolayer coverage of adsorbates on the single crystal surface. The temporal resolution of the instrument is limited by the CCD camera, which has a collection rate of 30 frames/s, while the spatial resolution is around 0.2 μm.

B. PEEM setup (FHI Berlin)

All experiments were carried out in a UHV vessel with a volume of about 60 l. The base pressure in the vessel was below 2×10^{-11} mbar. A gas inlet system with feedback-stabilization was used to keep the partial pressures of CO and oxygen constant during the experiments. The chamber was also equipped with an ion-gun for sputtering, facilities for LEED and Auger electron spectroscopy and two mass spectrometers, one of them differentially pumped to follow *in situ* the reaction rate of CO_2.

PEEM was used for imaging of adsorbate distributions on the single crystal surface. Its contrast is based on local differences in work function caused by different adsorbates and adsorbate coverages.[37] The surface is irradiated with UV light from a deuterium discharge lamp and the photoelectrons emitted from the sample surface are focused through three electrostatic lenses, intensified with a channel plate and finally made visible on a phosphorous screen. The spatial resolution of the PEEM used in the experiments is about 1 μm and the field of view on the sample is up to 750 μm. The

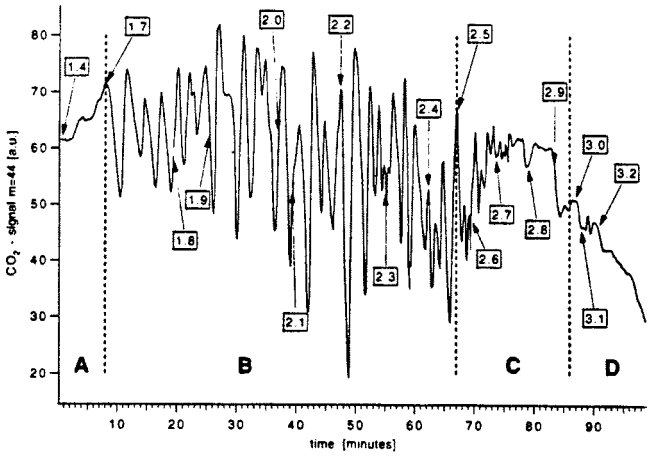

FIG. 1. Time series of the CO_2 production rate at 460 K for a constant oxygen pressure of 4×10^{-4} mbar. The numbers in the boxes denote the CO pressure in 10^{-5} mbar (Ref. 23).

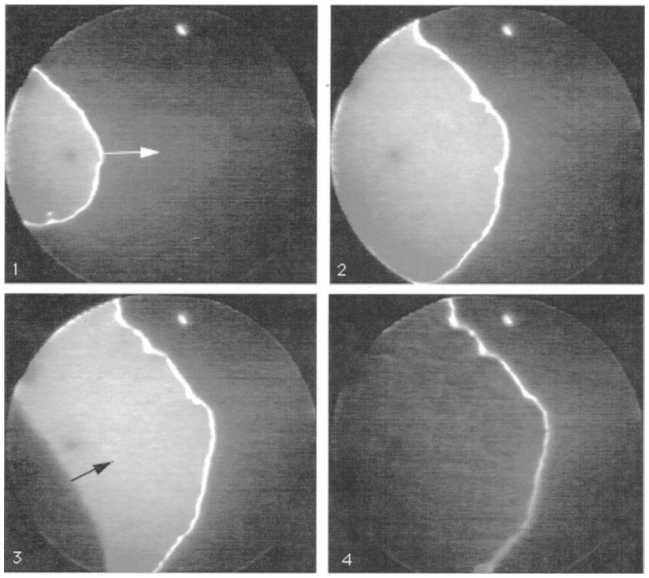

FIG. 2. PEEM image of CO front expanding into oxygen covered area, as denoted by the white arrow in frames 1 and 2. Frames 3 and 4 show an oxygen front extinguishing the newly formed CO-covered area (black arrow). $T=475$ K, the time difference between frames 1 and 2 and 2 and 3 is 15 s, the time difference between frames 3 and 4 is 2s, $p_{CO}=1.8\times10^{-5}$ mbar; $p_{O_2}=4\times10^{-4}$ mbar. The image diameter is 600 μm (Ref. 23).

temporal resolution of 20 ms is, as is the case of EMSI, limited by the video frequency recording the PEEM picture. According to the work functions of the clean Pt(100) surface (5.84 eV), the CO (6.0 eV) and the oxygen-covered surface (6.3 eV)[23] in the PEEM pictures oxygen covered areas appear dark and CO-covered domains are light gray.

IV. RESULTS AND DISCUSSION

A. Experiments at 10^{-4} mbar using PEEM

Spatio-temporal pattern formation was followed during the reaction at temperatures between 420 and 540 K, at variable CO pressure around 10^{-5} mbar and a fixed oxygen pressure of 4×10^{-4} mbar.[23] Between 420 and 510 K, irregular oscillations in the macroscopic reaction rate were observed (Fig. 1). At CO pressures of 1.7×10^{-5} mbar, for example, areas of CO nucleated on the otherwise fully oxygen-covered surface (Fig. 2), predominantly at defect sites. After growing to a size of up to 2 mm in diameter, the CO patch was rapidly filled up with oxygen again as shown in Fig. 2, frame 3. This transformed the surface back to the high reactivity state, and resulted in the reaction rate going through a maximum. With increasing CO pressure, the CO patches become larger and the amplitude of the oscillations goes up. Upon further increase of CO pressure, many small, irregular fronts began to develop, as can be seen in Fig. 3. Oxygen fronts fill the CO-covered areas and are immediately followed by new CO fronts. The reaction rate oscillations that were observed for lower CO pressures appear diminished and finally completely stop at a pressure of 3×10^{-5} mbar.

B. Experiments at 10^{-1} mbar using EMSI

In order to compare spatio-temporal pattern formation between low and high pressures on Pt(100), the reaction was also followed at a pressure of 8×10^{-2} mbar using EMSI.[38] Figure 4 shows the parameter space (defined by the CO/O_2 ratio and the corresponding sample temperature at a constant total pressure of 8×10^{-2} mbar) that produces spatio-temporal pattern formation and/or reaction rate oscillations (this can be compared to a parameter space for rate oscillations, reported by Eiswirth *et al.*[24]). Three distinct regions, marked by I, II and III in Fig. 4, exist where nonlinear phenomena could be observed. The first region [indicated by (I) in Fig. 4] is characterized by regular, large-amplitude oscillations in the production of CO_2 (Fig. 5). This type of behavior exists at temperatures between ~540 and 630 K, and at CO/O_2 ratios from 0.05 to 0.14. Such oscillations could never be observed at the aforementioned low-pressure stud-

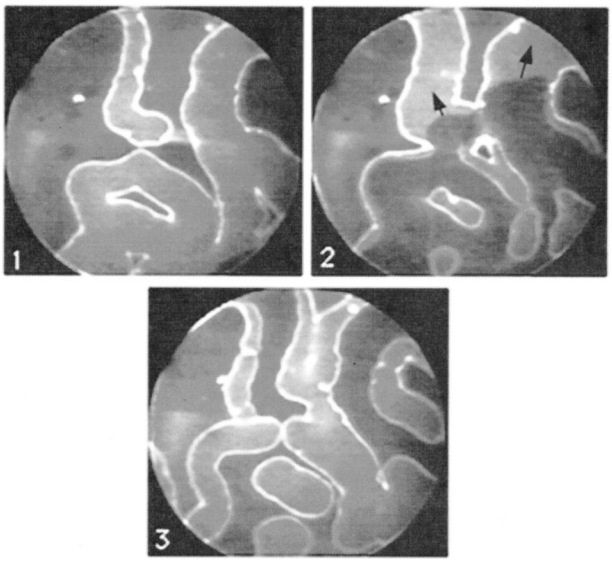

FIG. 3. PEEM image of irregular moving fronts on the Pt(100) surface at 4×10^{-4} mbar. $T=475$ K, $p_{CO}=3.6\times10^{-5}$ mbar; $p_{O_2}=4\times10^{-4}$ mbar. The time difference between the frames is 2 s. The image diameter is 600 μm (Ref. 23).

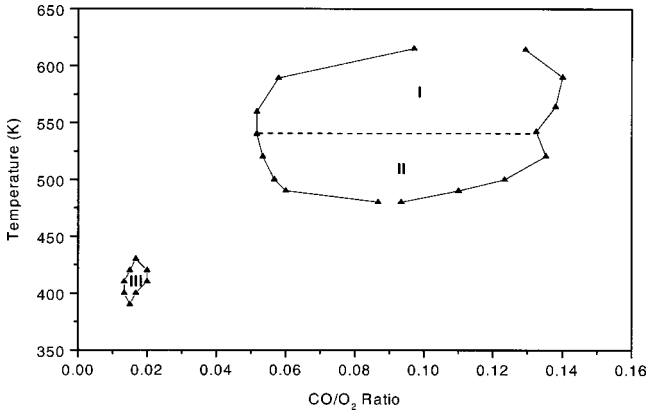

FIG. 4. Parameter space for nonlinear phenomena on Pt(100) for a total reactant pressure of 8×10^{-2} mbar. See text for explanation of regimes I–III (Ref. 38).

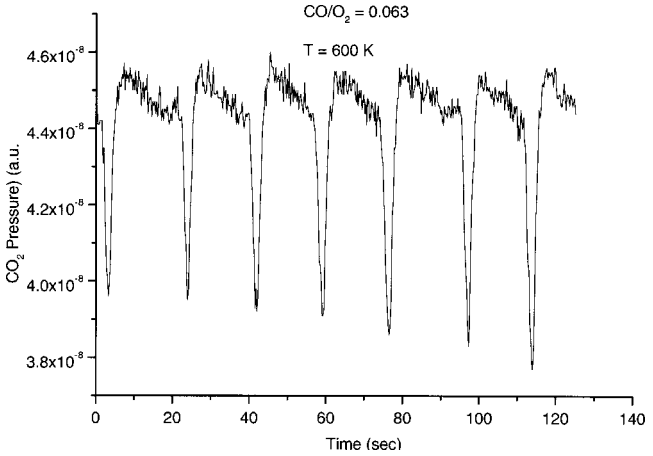

FIG. 6. Relaxation-type oscillations in region I at $T=600$ K and $CO/O_2=0.062$ (Ref. 38).

ies. The period and the shape of the oscillations remain constant even over hours of observation. EMSI reveals that in this region, transitions from the CO to the oxygen covered state and vice versa for periodic oscillations are spatially uniform and occur instantaneously. This is in contrast to the PEEM observations, where areas of CO and oxygen always coexist during rate oscillations. At the intermediate pressures, the surface flip-flops between states within 1/30 s. During oscillations in regime I, the entire single crystal is coupled efficiently through the gas phase. This results in synchronization of various areas, leading to well-defined reaction rate oscillations. This long range coupling mechanism is necessary for global rate oscillations and has also been reported for Pt (110) and polycrystalline platinum foils at lower pressures,[39,40] but it was never observed in the parameter space for oscillations during our measurements at lower pressures. Relaxation oscillations were also observed in regime I (Fig. 6). These oscillations, however, are now accompanied by distinct pattern formation. Transitions from the high reactive to the low reactive state are very fast (within one video frame) and spatially uniform. The reverse transition resulting in the return to the high reactive state, on the other hand, occurs via oxygen fronts forming on the predominantly CO covered surface and quickly spreading into the CO covered areas. Between transitions, the system now remains longer in the high reactive state, leading to the relaxation oscillations. Again, such oscillations could never be observed under low-pressure conditions.[23]

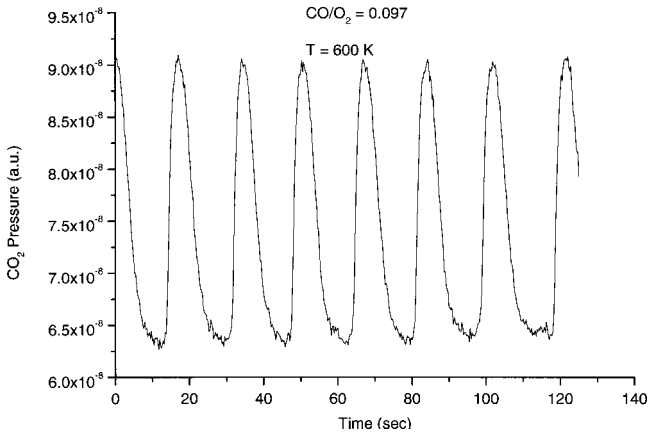

FIG. 5. Periodic rate oscillations in region I at $T=600$ K and $CO/O_2=0.097$ (Ref. 38).

Pattern formation without the presence of large-amplitude observable macroscopic rate oscillations characterizes the second regime (II). This phenomenon occurs between temperatures of 480 and 550 K. Figure 7 demonstrates one of the several types of patterns observed in this region. In the first six images, CO islands grow via slow moving CO fronts with velocities of $\sim25\ \mu$m/s. The last four images show a higher velocity oxygen front ($\sim250\ \mu$m/s) moving across the surface and transforming it back into the predominantly oxygen covered state.

The absence of measurable reaction rate oscillations can be explained as a result of the nature of the pattern formation. For global reaction rate oscillations to occur, the surface must undergo transitions in which the majority of the surface becomes primarily occupied by one adsorbate species, followed by a reverse transition during which the other adsorbate occupies the surface. When spatio-temporal patterns exist on the surface, such as in regime II, there are many areas present in either the high or low reactive state. This eliminates the possibility of macroscopic, large-amplitude rate oscillations. The coupling of different active areas on the catalyst surface in this region is governed mainly by local surface diffusion. The long range coupling mechanism, as proposed for regime I, is not very effective in regime II.

Spatio-temporal pattern formation was also observed in region III between 390 and 430 K, at considerably lower temperatures than the two other regions of pattern formation. Region III is not connected in the parameter space with regions I and II, i.e., for parameters between combined regions I and II and region III, no nonlinear phenomena could be observed. Periodic rate oscillations, similar to those seen in region I, were found to exist. However, the rate oscillations were not self-sustained indefinitely and typically ceased within several minutes. Figure 8 shows the variation of the reaction rate with the corresponding EMSI images, which show images at specific points during the oscillatory cycle. Eventually, reaction rate oscillations cease when a forward

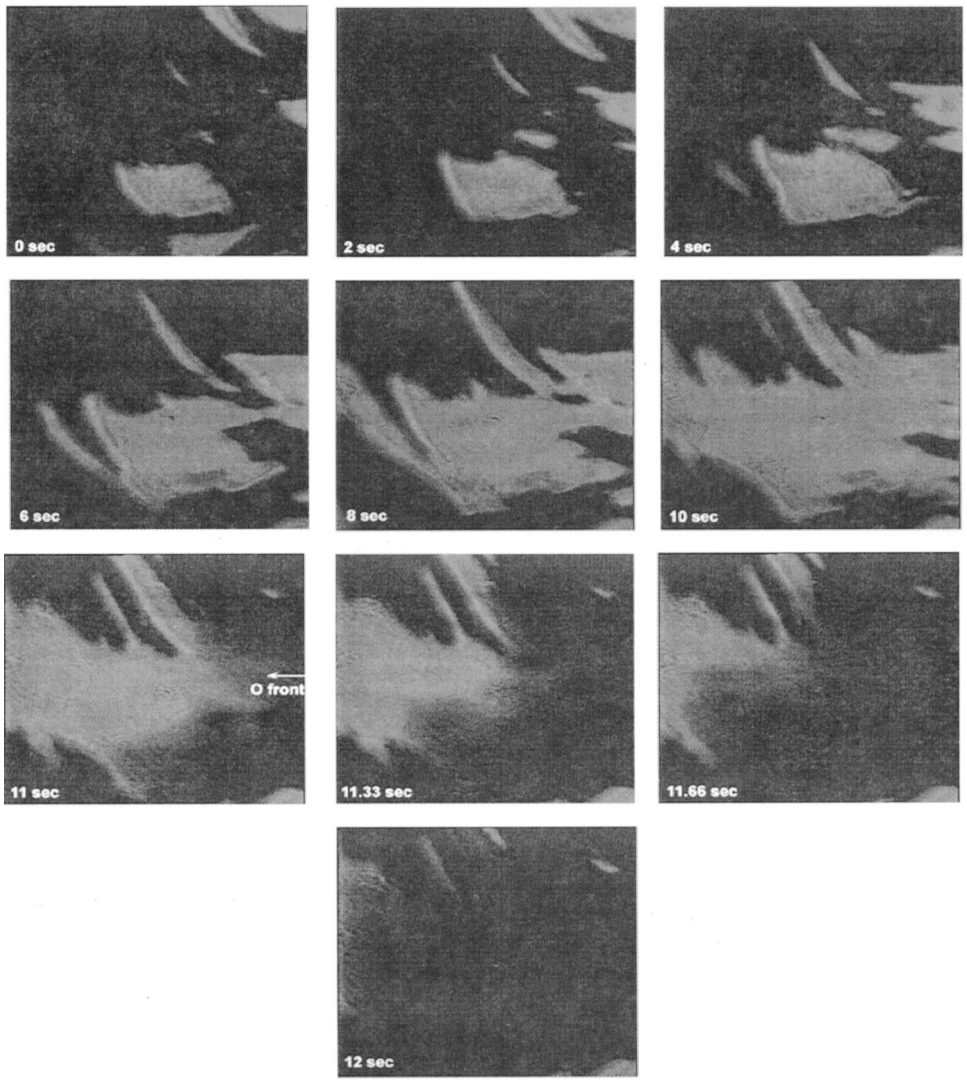

FIG. 7. Sequence of EMSI images (intervals of 2 s) of the Pt(100) surface in regime II at 520 K and $CO/O_2 = 0.09$. Oxygen covered areas appear darker while CO covered areas are lighter. The image size is $1 \times 1.25\ mm^2$ (Ref. 38).

transition to the CO covered state occurs and oxygen fronts are unable to reclaim the surface to produce the reverse transition, leaving the surface in a low reactive, CO covered state. The surface at intermediate pressures shows nonlinear phenomena at much lower temperatures in comparison to our low-pressure studies.[23]

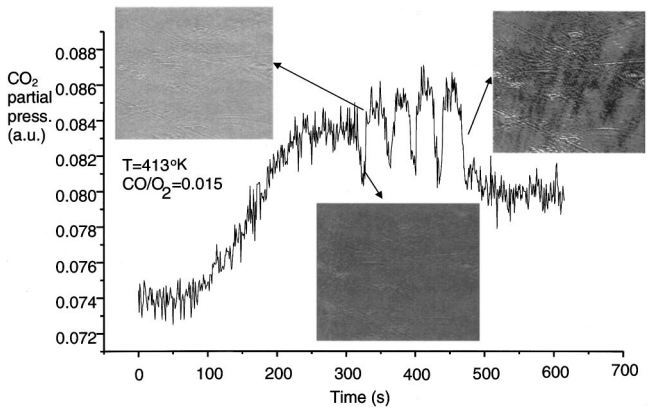

FIG. 8. Correlation between integral reaction rate oscillations and EMSI images of spatio-temporal pattern formation in regime III. $T = 410$ K and $CO/O_2 = 0.015$. The image size is $1 \times 1.25\ mm^2$ (Ref. 38).

C. Comparison of front velocities at low and intermediate pressures

Data showing corresponding velocities for oxygen and CO for the low-pressure regime is shown in Fig. 9, and data for the intermediate pressure regime is shown in Fig. 10. In both pressure regimes, the velocity of oxygen fronts decreases and that of CO fronts increases with an increase in the CO/O_2 ratio. At higher CO/O_2 ratios, CO adsorption dominates and leads to higher CO coverages on the surface. This restricts adsorption of oxygen, leading to a decrease in the front velocity of oxygen. Both CO and oxygen fronts show an increase in the front velocity with increasing catalyst temperature in the low as well as intermediate pressure regime, which is expected since the diffusion of adsorbates, in particular CO, on the surface increases with temperature. For all conditions, the oxygen fronts are faster than the CO fronts. PEEM experiments showed that the adsorbate coverage across oxygen fronts does not fall below the critical value necessary to initiate the surface phase transition from

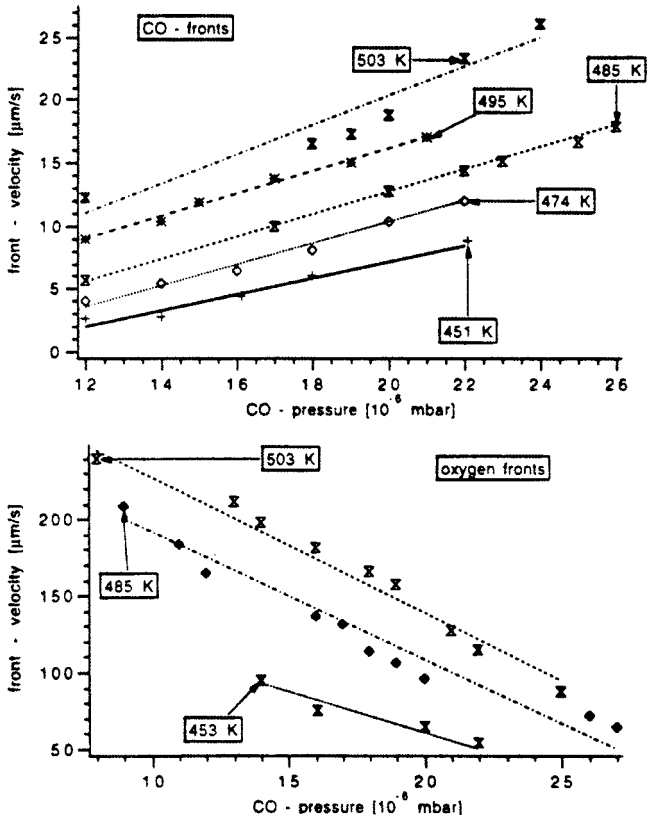

FIG. 9. CO and oxygen front velocities measured with PEEM at different temperatures for varying CO pressure and $p_{O_2}=4\times10^{-4}$ mbar (Ref. 23).

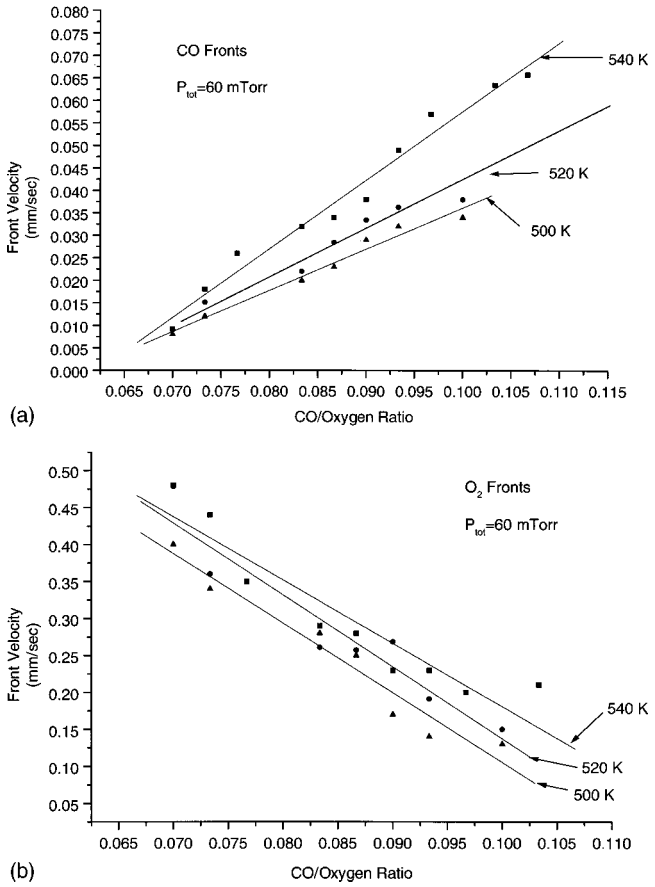

FIG. 10. (a) CO front velocities measured with EMSI in regime II at total pressure of 8×10^{-2} mbar for varying CO/O_2 ratios and different temperatures (Ref. 38). (b) Oxygen front velocities measured with EMSI in regime II at total pressure of 8×10^{-2} mbar for varying CO/O_2 ratios and different temperatures (Ref. 38).

the 1×1 phase to the hex phase.[23,41,42] For CO fronts, however, the coverage at the reaction interface does become low enough to initiate the surface phase transition,[23] thereby slowing down CO fronts compared to oxygen fronts. In addition, the difference in adsorption probabilities and the impingement rates also adds to the difference in front velocities. At intermediate pressures, both CO and oxygen front velocities were 1.5 to 2 times higher than those measured at low pressures. Front velocities reached values up to 500 μm/s for oxygen fronts and up to 40 μm/s for CO fronts, thus coupling large areas of the single crystal surface very efficiently. This could also be the reason why the oscillations at intermediate pressures are more regular compared to those at lower pressures. Also, at higher pressures, higher fractional coverages are expected on the surface, leading to higher reaction rates between CO and adjoining oxygen, hence the amplitude of oscillations at intermediate pressures are higher.

D. Formation of subsurface oxygen

During the low-pressure experiments and for temperatures of above 540 K, no self-sustained rate oscillations could be observed in CO_2 production. At these elevated temperatures, the formation of a less reactive oxygen species with low work function was observed during pattern formation (Fig. 11).[23] When a CO front moves along an oxygen-covered surface, the edge of the front appears brighter than both the CO covered surface and the clean surface, i.e., this species has a work function lower than the clean metallic surface, and hence can be easily distinguished from chemisorbed oxygen, which appears much darker in the PEEM. Spectroscopic evidence for the existence of subsurface oxygen was obtained using Auger electron spectroscopy.[14] The

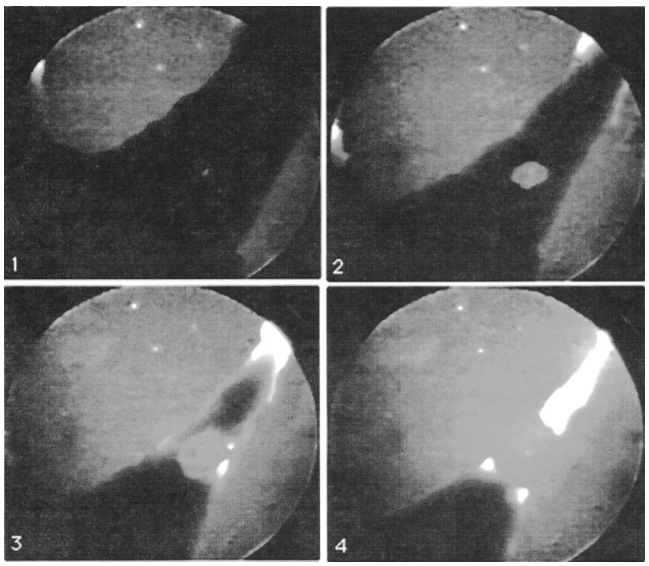

FIG. 11. Change from chemisorbed oxygen, which appears dark in the PEEM, to subsurface oxygen, which appears very bright in the PEEM, under reaction conditions. $T=543$ K; $p_{O_2}=4\times10^{-4}$ mbar; $p_{CO}=2.50\times10^{-5}$ mbar. The time difference between the frames is 40 s (Ref. 23).

formation of this subsurface species of oxygen was investigated systematically, and it could be formed under controlled conditions when heating oxygen islands surrounded by an adlayer of CO to 650 K.[13] The transformation of chemisorbed oxygen to subsurface oxygen was characterized by an activation energy of ~ 15 kcal/mole. It was concluded that 1×1 areas adjoining hex areas are needed for the formation of the subsurface oxygen. The subsurface oxygen once formed was found stable, but could be removed by heating the crystal to temperatures of 750 K, about 100 K higher than the desorption temperature of chemisorbed oxygen. The subsurface oxygen could also be removed by exposing it to CO, although this is a slow process compared to direct reaction between CO and oxygen.[13] This suggests that CO adsorption causes the subsurface oxygen to diffuse from the subsurface state and then undergo reaction with CO; this could be attributed to a rearrangement of atoms caused by CO adsorption. Oxygen adsorption is largely inhibited on subsurface oxygen.

We believe that subsurface oxygen also plays an important part in the feedback mechanism for self-sustained rate oscillations observed at intermediate and higher pressures. We base this on the following reasoning: subsurface oxygen has been observed at temperatures between 520 and 540 K (the upper portion of the temperature window) during oscillations at lower pressures with the PEEM. At intermediate pressures, the temperature window for oscillations is seen to shift to high temperatures of around 600 K. The local coverage of adsorbates is high enough to ensure that most of the catalyst is in the 1×1 phase. This suggests that the phase transition may no longer be the feedback mechanism for oscillations, and the less reactive subsurface oxygen species could become the driving force for the oscillations. This needs to be experimentally explored more, however. EMSI, in principle, can be used to detect contrast between subsurface oxygen and chemisorbed species by preparing subsurface oxygen islands on the surface. Recent experiments in our laboratory have shown that the contrast between chemisorbed species and subsurface oxygen is very small and therefore it will be difficult to detect the presence of subsurface oxygen during reaction at intermediate pressures. Recent modeling efforts in our group have shown that the formation of subsurface oxygen at intermediate pressures can indeed explain the presence of regular reaction rate oscillations without the need for an adsorbate induced surface phase transition.[43] This model is on similar lines to that by Sales *et al.*,[12] who proposed a model based on oxide formation to explain oscillations in the atmospheric pressure regime.

V. SUMMARY

CO oxidation on Pt(100) was investigated at reactant pressures ranging from 10^{-4} to 10^{-1} mbar using photoemission electron microscopy and ellipsomicroscopy for surface imaging to monitor spatio-temporal pattern formation on the catalyst surface and mass spectrometry to monitor the integral reaction rate. Only irregular oscillations accompanied by formation of CO islands on an oxygen-covered surface were observed with the PEEM at pressures in the 10^{-5} mbar range; no spatially uniform transitions were detected. The formation of subsurface oxygen was detected at these pressures using PEEM. At 10^{-2} mbar, three distinct temperature regions showing nonlinear phenomena were observed. The first region, at temperatures between 540 and 615 K, is characterized by macroscopic, regular reaction rate oscillations with spatially uniform, instantaneous transitions between CO and oxygen covered states. The second region exists at temperatures between 480 and 540 K and exhibits continuous dynamic pattern formation with no visible macroscopic kinetic oscillations. The third region exists at temperatures between 390 and 430 K and is characterized by macroscopic rate oscillations, which continue for several oscillation periods and then cease with the onset of pattern formation.

Detailed measurements at both low and intermediate pressures have thus successfully bridged the pressure gap that has existed for a number of years for CO oxidation on Pt(100). Clearly, there is a significant change in the period, the shape and type of rate oscillations as well as the type of pattern formation from low to intermediate pressures. It is possible that phase transition may no longer be the driving force for rate oscillations in this system. There is a need to now investigate phenomena at higher (atmospheric and above) pressures, to investigate the possibility of pattern formation or rate oscillations and to possibly draw correlations with supported catalysts under similar conditions.

ACKNOWLEDGMENTS

We would like to thank G. Ertl, H. H. Rotermund, K. Asakura, T. D. Pletcher, and J. Dicke for many fruitful discussions and for performing many of the experiments. Part of this work was funded by the National Science Foundation (Grant No. CTS-9733821).

[1] G. Ertl, Surf. Sci. **287**, 1 (1993).
[2] T. Engel and G. Ertl, J. Chem. Phys. **69**, 1267 (1978).
[3] H. H. Rotermund, Surf. Sci. Rep. **29**, 265 (1997).
[4] M. D. Graham, I. G. Kevrekidis, K. Asakura, J. Lauterbach, K. Krischer, H. H. Rotermund, and G. Ertl, Science **264**, 80 (1994).
[5] G. Ertl and H. H. Rotermund, Curr. Opin. Solid State Mater. Sci. **1**, 617 (1996).
[6] R. Imbihl and G. Ertl, Chem. Rev. **95**, 697 (1995).
[7] M. Eiswirth, M. Bar, and H. H. Rotermund, Physica D **84**, 40 (1995).
[8] G. Ertl, Surf. Sci. **152**, 328 (1985).
[9] M. P. Cox, G. Ertl, R. Imbihl, and J. Rustig, Surf. Sci. **134**, L517 (1983).
[10] A. Hopkinson and D. A. King, Faraday Discuss. **96**, 255 (1993).
[11] M. Stiles and H. Metiu, Chem. Phys. Lett. **128**, 337 (1986).
[12] B. C. Sales, J. E. Turner, and M. B. Maple, Surf. Sci. **114**, 381 (1982).
[13] J. Lauterbach, K. Asakura, and H. H. Rotermund, Surf. Sci. **313**, 52 (1994).
[14] H. H. Rotermund, J. Lauterbach, and G. Haas, Appl. Phys. A: Solids Surf. **57**, 507 (1993).
[15] S. Ladas, R. Imbihl, and G. Ertl, Surf. Sci. **219**, 88 (1989).
[16] R. J. Behm, P. A. Thiel, P. R. Norton, and G. Ertl, J. Chem. Phys. **78**, 7437 (1983).
[17] P. A. Thiel, R. J. Behm, P. R. Norton, and G. Ertl, J. Chem. Phys. **78**, 7448 (1983).
[18] M. A. Barteau, E. I. Ko, and R. J. Madix, Surf. Sci. **102**, 99 (1981).
[19] Y. Y. Yeo, L. Vattuone, and D. A. King, J. Chem. Phys. **104**, 3810 (1996).
[20] M. Kim, W. S. Sim, and D. A. King, J. Chem. Soc., Faraday Trans. **92**, 4781 (1996).

[21] M. Gruyters, T. Ali, and D. A. King, J. Phys. Chem. **100**, 14417 (1996).
[22] J. Lauterbach, Ph.D., Free University, 1994.
[23] J. Lauterbach and H. H. Rotermund, Surf. Sci. **311**, 231 (1994).
[24] M. Eiswirth, R. Schwankner, and G. Ertl, Z. Phys. Chem., Neue Folge **144**, 59 (1985).
[25] M. P. Cox, G. Ertl, and R. Imbihl, Phys. Rev. Lett. **54**, 1725 (1985).
[26] H. H. Rotermund, Electron Microscopy and Analysis 1995, Proceedings of the Institute of Physics Electron Microscopy and Analysis Group Conference (1995), p. 215.
[27] H. H. Rotermund, Electr. Spectr. Rel. Phen. **98-99**, 41 (1997).
[28] H. H. Rotermund, W. Engel, S. Jakubith, A. Vonoertzen, and G. Ertl, Ultramicroscopy **36**, 164 (1991).
[29] H. H. Rotermund, G. Haas, R. U. Franz, R. M. Tromp, and G. Ertl, Science **270**, 608 (1995).
[30] H. H. Rotermund, G. Haas, R. U. Franz, R. M. Tromp, and G. Ertl, Appl. Phys. A: Mater. Sci. Process. **61**, 569 (1995).
[31] J. Dicke, H. H. Rotermund, and J. Lauterbach, J. Opt. Soc. Am. A Opt. Image Sci. Vis **17**, 135 (2000).
[32] G. Haas, T. D. Pletcher, G. Bonilla, T. A. Jachimowski, H. H. Rotermund, and J. Lauterbach, J. Vac. Sci. Technol. A **16**, 1117 (1998).
[33] G. Haas, Freie Universitat, 1997.
[34] J. Dicke, H. H. Rotermund, and J. Lauterbach, Surf. Sci. **454**, 352 (2000).
[35] J. Lauterbach, G. Bonilla, and T. D. Pletcher, Chem. Eng. Sci. **54**, 4501 (1999).
[36] T. A. Jachimowski and J. Lauterbach, Rev. Sci. Instrum. **69**, 2757 (1998).
[37] W. Engel, M. E. Kordesch, H. H. Rotermund, S. Kubala, and A. von Oertzen, Ultramicroscopy **36**, 148 (1991).
[38] T. P. Lele, T. D. Pletcher, and J. Lauterbach, AIChE J. **47**, 1418 (2001).
[39] J. Lauterbach and H. H. Rotermund, Catal. Lett. **27**, 27 (1994).
[40] S. Jakubith, H. H. Rotermund, W. Engel, A. von Oertzen, and G. Ertl, Phys. Rev. Lett. **65**, 3013 (1990).
[41] W. Swiech, C. S. Rastomjee, R. Imbihl, J. W. Evans, B. Rausenberger, W. Engel, A. K. Schmid, A. M. Bradshaw, and E. Zeitler, Surf. Sci. **307-309**, 138 (1994).
[42] B. Rausenberger, W. Swiech, C. S. Rastomjee, M. Mundschau, W. Engel, E. Zeitler, and A. M. Bradshaw, Chem. Phys. Lett. **215**, 109 (1993).
[43] T. P. Lele and J. Lauterbach (in preparation).